Robotics and Autonomous Systems 66 (2015) 64–74

Contents lists available at ScienceDirect

Robotics and Autonomous Systems

journal homepage: www.elsevier.com/locate/robot

Passivity-based visual feedback control with dynamic compensation of mobile manipulators: Stability and L_2-gain performance analysis

Víctor H. Andaluz [a], Flavio Roberti [b,c,*], Lucio Salinas [b,c], Juan M. Toibero [b,c], Ricardo Carelli [b,c]

[a] Universidad Técnica de Ambato, Av. Colombia y Chile, Ambato, Ecuador

[b] Instituto de Automática, Universidad Nacional de San Juan - CONICET, Av. San Martín Oeste 1109 (J5400ARL), San Juan, Argentina

[c] Consejo Nacional de Investigaciones Científicas y Técnicas (CONICET), Argentina

HIGHLIGHTS

- We address the problem of visual control to solve the target tracking problem.
- We consider both the kinematic and dynamic models in the control system design.
- The design of the stable control system is based on its passivity properties.
- A robustness analysis and an L_2-gain performance analysis are also presented.
- Simulations and experimental results are shown to verify the system's performance.

ARTICLE INFO

Article history:
Received 5 October 2012
Received in revised form
30 July 2014
Accepted 3 December 2014
Available online 22 January 2015

Keywords:
Mobile manipulator
Passivity based control
Non-linear control
Visual servoing

ABSTRACT

This paper addresses the problem of visual dynamic control based on passivity to solve the target tracking problem of mobile manipulators with eyes-in-hand configuration in the 3D-workspace. The redundancy of the system is used for obstacles avoidance and singular configuration prevention through the system's manipulability control. The design of the stable control system is based on its passivity properties. A robustness analysis and an L_2-gain performance analysis are also presented. Finally, simulation and experimental results are reported to verify the stability and L_2-gain performance of the dynamic visual feedback system.

1. Introduction

Mobile manipulator is nowadays a widespread term that refers to robots built by a robotic arm mounted on a mobile platform. This kind of system, which is usually characterized by a high degree of redundancy, combines the manipulability of a fixed-base manipulator with the mobility of a wheeled platform, thus allowing the most usual missions of robotic systems which require both locomotion and manipulation abilities. They offer multiple applications in different industrial and productive areas such as mining and construction or for people assistance [1,2].

Recently, some authors have proposed to integrate visual servoing into mobile robots for grasping or manipulation tasks [3–6], as well as for solving vision based tracking problem [7–9], resulting in vision-based autonomous mobile manipulation systems. Additionally, researchers proposed the using of a path-planning algorithm along with a reactive visual servoing strategy. The planning stage takes into account different critical constraints or system uncertainties, obtaining a more robust visual based control system. A comprehensive survey about mixing path-planning algorithms with reactive visual servoing strategies can be found in [10].

Among the most relevant works, in [3] authors present a framework of hand–eye relation for visual servoing with global view and mobility. Two mobile manipulators are used: for the main robot the camera architecture is an eye-to-hand configuration,

* Corresponding author at: Instituto de Automática, Universidad Nacional de San Juan - CONICET, Av. San Martín Oeste 1109 (J5400ARL), San Juan, Argentina. Tel.: +54 264 4213303; fax: +54 264 4213672.

E-mail addresses: victorhandaluz@uta.edu.ec (V.H. Andaluz), froberti@inaut.unsj.edu.ar (F. Roberti), lsalinas@inaut.unsj.edu.ar (L. Salinas), mtoibero@inaut.unsj.edu.ar (J.M. Toibero), rcarelli@inaut.unsj.edu.ar (R. Carelli).

http://dx.doi.org/10.1016/j.robot.2014.12.009
0921-8890/

and for the second robot it is selected as eye-in-hand. Ref. [4] presents a robust vision-based mobile manipulation system for wheeled mobile robots, addressing the retention of visual features in the field of view of the camera. A hybrid controller for mobile manipulation is developed to integrate the image based visual servoing controller and the Q-learning controller through a rule-based supervisor. In [7] it has developed an image-based visual servo controller for non-holonomic mobile manipulators. Two well-known methods of redundancy resolution for fixed-base manipulators are extended for kinematics modeling of a specific non-holonomic mobile manipulator. The proposed approach is illustrated only through computer simulation.

Frequently, theoretical analysis about the stability of the servo visual control system is based on Lyapunov theory [3,11]. An alternative choice is a passivity-based analysis [12–14], which has been typically used in the analysis of robotic manipulators control systems [15–19]. A few recent works report control algorithms for mobile robots based on passivity theory [20–22], for coordinate multi-robots systems [23–25], and even the locomotion problem of biped robots has been addressed using passivity theory [26]. Closer to our work, passivity properties have been also used in order to design control systems for mobile manipulators [27, 28], and specifically in vision based tracking control for mobile platforms [22]. However, from the best of our knowledge, vision based stable controllers for mobile manipulators using passivity properties have not been reported yet.

In this paper it is presented an image based visual servo controller with dynamic compensation, designed for 3D target tracking by mobile manipulators with eye-in-hand configuration. The control system design as well as the stability proof and the robustness analysis are based on its passivity properties and the input–output systems theory. With this aim, it is considered a robotic arm mounted on a non-holonomic mobile platform which dynamic model [29] has reference velocities as input signals as it is common in commercial robots. The redundancy of this mobile manipulator is effectively used for the achievement of two additional objectives: the capability to avoid obstacles in the platform path and the prevention of singular configurations.

The design of the controller is based on two parts, each one being a controller itself. The first one is a minimum norm visual servo controller which avoids saturations of the velocity commands. It is based on both the mobile manipulator's kinematic model and the vision system model. The second one is a dynamic compensation controller, which receives as inputs the velocity references calculated by the kinematic controller. Based on the passivity properties and the input–output systems theory, the convergence to zero of the control errors is proved considering perfect knowledge of the object's velocity. Then, a robustness analysis considering errors in the object velocity estimation is performed, concluding that control errors are ultimately bounded. Additionally, L_2-gain performance is proved when the control errors reach the final bound. To validate the proposed control algorithms, experimental results are included and discussed.

The paper is arranged into six sections. Section 2 presents the kinematic model of the camera-robot system and the dynamic model of the robot. The problem formulation and the design of the vision-based controller for the mobile manipulator are presented in Section 3. A robustness analysis and L_2-gain performance analysis are presented in Section 4. The experimental results are presented and discussed in Section 5. Finally, conclusions are given in Section 6.

2. System models

2.1. Dynamic model of the mobile manipulator

The mathematical model that represents the dynamics of a mobile manipulator considered in this work is derived from the one presented in [30]. The only difference is the inclusion of PD-like low level velocity controllers for the actuators. This way, a dynamic model with velocity references as input is obtained [29],

$$\mathbf{M}(\mathbf{q})\,\dot{\mathbf{v}} + \mathbf{C}(\mathbf{q},\mathbf{v})\,\mathbf{v} + \mathbf{g}(\mathbf{q}) = \mathbf{v}_{\mathbf{ref}} \tag{1}$$

where $\mathbf{v}$ is the vector of mobile manipulator velocities which contains the linear and angular velocities of the mobile platform and the joint velocities of the robotic arm, $\mathbf{M}(\mathbf{q}) \in \mathbb{R}^{n\times n}$ is a positive definite matrix, $\mathbf{C}(\mathbf{q},\mathbf{v})\,\mathbf{v} \in \mathbb{R}^n$, $\mathbf{g}(\mathbf{q}) \in \mathbb{R}^n$, and $\mathbf{v}_{\mathbf{ref}} \in \mathbb{R}^n$ is the vector of velocity input signals, whereas $\mathbf{q} = \begin{bmatrix} q_1 & q_2 & \cdots & q_m \end{bmatrix}^T = \begin{bmatrix} \mathbf{q}_p^T & \mathbf{q}_a^T \end{bmatrix}^T \in \mathbb{R}^m$ represents the generalized coordinates of the mobile manipulator, where $\mathbf{q}_p \in \mathbb{R}^{mp}$ and $\mathbf{q}_a \in \mathbb{R}^{ma}$ represent the generalized coordinates of the mobile platform and for the robotic arm, respectively. More details about the dynamic model (1) can be found in [29].

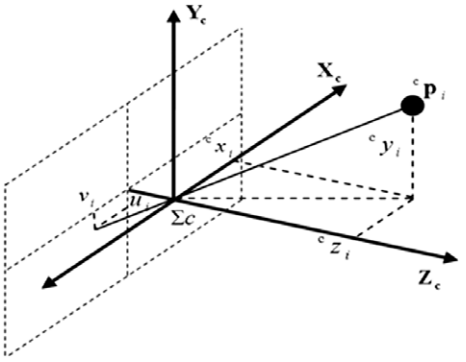

Fig. 1. Pinhole camera model.

2.2. Camera projection model

This work considers a vision camera located at the end-effector of the robotic arm. The model used in this paper is the perspective projection model (*pinhole model*), shown in Fig. 1.

Let f_c be a focal length, ${}^w\mathbf{p}_i \in \mathbb{R}^3$ and ${}^c\mathbf{p}_i = \begin{bmatrix} {}^cx_i & {}^cy_i & {}^cz_i \end{bmatrix}^T \in \mathbb{R}^3$ be the 3D position vectors of the target's ith object point, relative to Σo and Σc, respectively. Σo represents the world framework and Σc is the camera framework.

The perspective projection of the ith object point onto the image plane gives us the ith image feature vector $\boldsymbol{\xi}_i = \begin{bmatrix} u_i & v_i \end{bmatrix}^T \in \mathbb{R}^2$ as

$$\boldsymbol{\xi}_i\left({}^cx_i, {}^cy_i, {}^cz_i\right) = -\frac{f_c}{{}^cz_i}\begin{bmatrix} {}^cx_i \\ {}^cy_i \end{bmatrix}. \tag{2}$$

This work considers a moving target formed by two vertically aligned spheres with known diameter D, and the image feature vector is defined as $\boldsymbol{\xi} = \begin{bmatrix} u_1 & v_1 & v_2 \end{bmatrix}^T$ (Fig. 2). Then, the following equation represents the vision system when the target object moves with finite velocity ${}^w\dot{\mathbf{p}}$,

$$\dot{\boldsymbol{\xi}} = \mathbf{J}\left(\mathbf{q}, \boldsymbol{\xi}, {}^cz\right)\mathbf{v} + \mathbf{J_o}\left(\mathbf{q}, \boldsymbol{\xi}, {}^cz\right){}^w\dot{\mathbf{p}} \tag{3}$$

where $\mathbf{v}$ represents a vector containing the linear and angular velocities of the mobile platform and the joints velocities of the robotic arm; $\mathbf{J}$ and $\mathbf{J_o}$ represent the total Jacobian matrix and the object Jacobian matrix. Note that $\mathbf{J}$ includes not only the kinematic models of both the mobile platform (with its non-holonomic constraint) and the robotic arm, but also the image Jacobian of the vision camera.

It is important to remark that it is necessary to have additional information about the target in order to calculate the Jacobian matrices. This work considers the physical dimension D of the

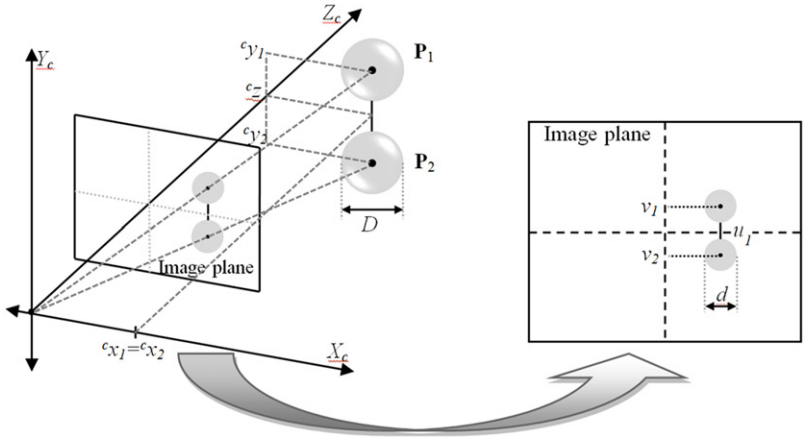

Fig. 2. Image features.

target (diameter of the spheres) as known for the calculus of ^cz_i. For the sake of simplicity, from now on we will use of the following notation:

$$\mathbf{J} = \mathbf{J}\left(\mathbf{q}, \xi, {}^cz\right), \qquad \mathbf{J_o} = \mathbf{J_o}\left(\mathbf{q}, \xi, {}^cz\right) \quad \text{and} \quad \dot{\mathbf{p}} = {}^w\dot{\mathbf{p}}.$$

3. Passivity-based controllers design

This section presents the design of a visual controller to make a mobile manipulator capable to track a moving object on the 3D space, making the image features error $\tilde{\boldsymbol{\xi}}(t) = \boldsymbol{\xi}(t) - \boldsymbol{\xi}_d$ converge to zero. This way, the control objective is formally defined as follows,

$$\lim_{t\to\infty} \tilde{\boldsymbol{\xi}}(t) = \mathbf{0}.$$

First, a minimum norm kinematics-based controller is designed and the convergence to zero of the image features error is proved considering perfect velocity tracking and perfect knowledge about the velocity of the moving object. Then, a more realistic situation is considered when a velocity error appears, and a dynamics-based controller is designed to verify the convergence to zero of the image features error under this condition.

In order to cope with the above mentioned control objectives, it is proposed a novel control algorithm and it is shown how the passivity properties of the control system described in Fig. 3 allow proving the asymptotic convergence of the feature errors to zero.

3.1. Passivity property of the vision system

First the passivity property of the vision system will be proved for a moving object, i.e., $\dot{\mathbf{p}} \neq \mathbf{0}$. Taking the energy function $V_\xi = \frac{1}{2}\boldsymbol{\xi}^T\boldsymbol{\xi}$, its time derivative is,

$$\dot{V}_\xi = \frac{1}{2}\boldsymbol{\xi}^T\dot{\boldsymbol{\xi}} = \boldsymbol{\xi}^T\left(\mathbf{J}\mathbf{v} + \mathbf{J}_o\dot{\mathbf{p}}\right) \tag{4}$$

and integrating on the interval $[0, T]$ the following expression is obtained,

$$\int_0^T \dot{V}_\xi dt = \int_0^T \boldsymbol{\xi}^T\left(\mathbf{J}\mathbf{v} + \mathbf{J}_o\dot{\mathbf{p}}\right) dt. \tag{5}$$

Now, consider $\mathbf{J}^\# = \mathbf{W}^{-1}\mathbf{J}^T\left(\mathbf{J}\mathbf{W}^{-1}\mathbf{J}^T\right)^{-1}$ the right pseudo-inverse matrix of $\mathbf{J}$, with $\mathbf{W}$ a positive definite matrix, and assume that matrix $\mathbf{J}$ is outside the singularity points. Then, (5) can be rewritten as,

$$\begin{aligned}\int_0^T \boldsymbol{\xi}^T\left(\mathbf{J}\mathbf{v} + \mathbf{J}_o\dot{\mathbf{p}}\right) dt &= \int_0^T \left(\mathbf{J}^T\boldsymbol{\xi}\right)^T\left(\mathbf{v} + \mathbf{J}^\#\mathbf{J}_o\dot{\mathbf{p}}\right) dt \\ &= V_\xi(T) - V_\xi(0) \geq -V_\xi(0).\end{aligned} \tag{6}$$

Hence, it can be concluded that the mapping $\left(\mathbf{v} + \mathbf{J}^\#\mathbf{J}_o\dot{\mathbf{p}}\right) \rightarrow \left(\mathbf{J}^T\boldsymbol{\xi}\right)$ is passive [12]. This mapping represents the vision system considering as parts of the system input both the robot velocities $\mathbf{v}$ and the target velocity $\dot{\mathbf{p}}$, and the features vector as the system output.

3.2. Kinematic controller design

Considering now the image features error $\tilde{\boldsymbol{\xi}}(t) = \boldsymbol{\xi}(t) - \boldsymbol{\xi}_d$ instead of the image features $\boldsymbol{\xi}(t)$ in order to take into account the regulation problem on the image plane, the passivity property of the vision system holds. Notice that a regulation problem in the image plane, considering a moving target, implies a tracking problem in the 3D workspace. This passivity property is proved by considering the following positive definite function,

$$V_1 = \int_0^{\tilde{\xi}} \eta^T\mathbf{K_c}(\eta)\, d\eta \tag{7}$$

and its time derivative on the trajectories of the system,

$$\dot{V}_1 = \tilde{\boldsymbol{\xi}}^T\mathbf{K_c}\left(\tilde{\boldsymbol{\xi}}\right)\dot{\tilde{\boldsymbol{\xi}}} = \tilde{\boldsymbol{\xi}}^T\mathbf{K_c}\left(\tilde{\boldsymbol{\xi}}\right)\left[\mathbf{J}\mathbf{v} + \mathbf{J}_o\dot{\mathbf{p}}\right] \tag{8}$$

where $\mathbf{K_c}\left(\tilde{\boldsymbol{\xi}}\right) = \text{diag}\left(\frac{k_i}{1+|\tilde{\xi}_i|}\right) \in \mathbb{R}^{r\times r}$ is a symmetric and positive definite gain matrix with $k_i > 0$, and $i = 1, 2, \ldots, r$. It is said that $\mathbf{K_c}\left(\tilde{\boldsymbol{\xi}}\right) \in \mathbb{R}^{r\times r}$ when considering a general case where $\boldsymbol{\xi} \in \mathbb{R}^r$.

Integrating V_1 on the interval $[0, T]$ it is obtained,

$$\begin{aligned}&\int_0^T \dot{V}_1 dt = \int_0^T \tilde{\boldsymbol{\xi}}^T\mathbf{K_c}\left(\tilde{\boldsymbol{\xi}}\right)\left[\mathbf{J}\mathbf{v} + \mathbf{J}_o\dot{\mathbf{p}}\right] dt = V_1(T) - V_1(0) \\ &\int_0^T \nu_{\tilde{\xi}}^T\left[\mathbf{v} + \mathbf{J}^\#\mathbf{J}_o\dot{\mathbf{p}}\right] dt \geq -V_1(0)\end{aligned} \tag{9}$$

where $\nu_{\tilde{\xi}} = \mathbf{J}^T\mathbf{K_c}\left(\tilde{\boldsymbol{\xi}}\right)\tilde{\boldsymbol{\xi}}$. Thus, it can be concluded that mapping $\left[\mathbf{v} + \mathbf{J}^\#\mathbf{J}_o\dot{\mathbf{p}}\right] \rightarrow \nu_{\tilde{\xi}}$ is passive.

Now, the following control law is proposed for 3D target tracking on the work space by a mobile manipulator system with eye-in-hand configuration, based on the error on the image plane and the mobile manipulator's redundancy

$$\mathbf{u} = -\nu_{\tilde{\xi}} - \mathbf{J}^\#\mathbf{J}_o\dot{\mathbf{p}} + \left(\mathbf{I} - \mathbf{J}^\#\mathbf{J}\right)\boldsymbol{k_1}\tanh\left(\boldsymbol{k_2}\boldsymbol{\Lambda}\right) \tag{10}$$

where $\mathbf{u} = \begin{bmatrix}u_c & \omega_c & \dot{\theta}_{1c} & \dot{\theta}_{2c} & \cdots & \dot{\theta}_{mac}\end{bmatrix}^T$ is the kinematic control vector for the mobile manipulator. The third term in (10) defines self-motion of the mobile manipulator in which the matrix

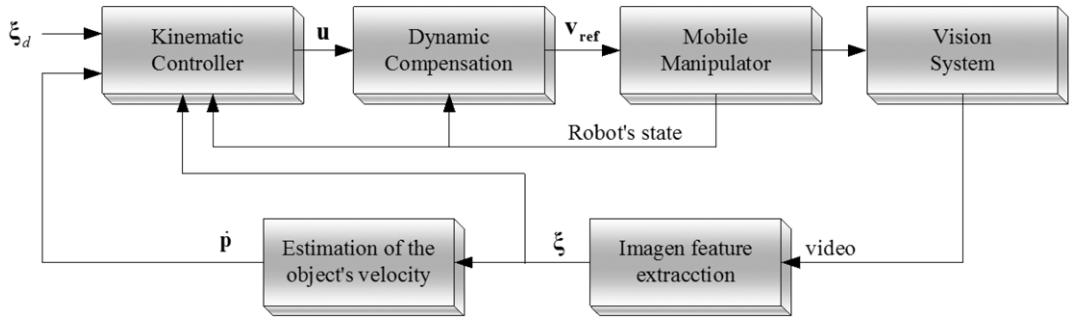

Fig. 3. Dynamic visual control for 3D target tracking of mobile manipulators.

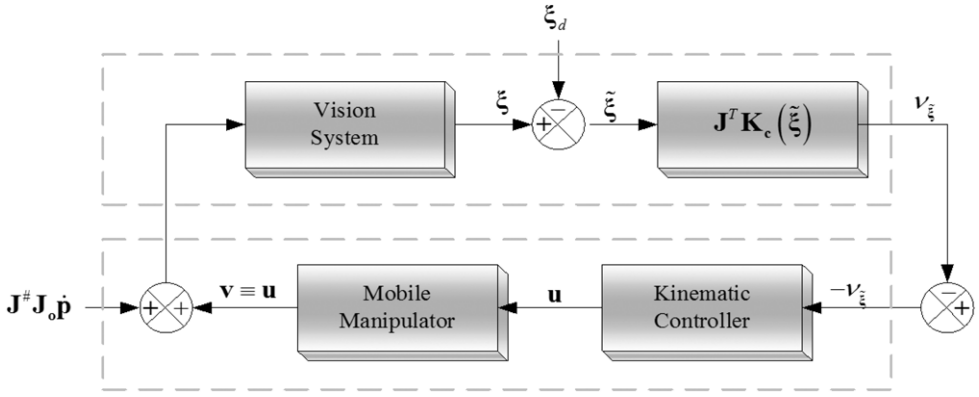

Fig. 4. Kinematic control system block diagram.

$\left(\mathbf{I}-\mathbf{J}^{\#}\mathbf{J}\right)$ projects the arbitrary vector $\mathbf{\Lambda}$ onto the null space of the Jacobian matrix $\mathbf{J}$, where $\boldsymbol{k_1}\mathbb{R}^{n\times n}$ and $\boldsymbol{k_2} \in \mathbb{R}^{n\times n}$ are positive definite diagonal gain matrices, and $\mathbf{\Lambda}$ is an arbitrary vector which contains the velocities associated to the mobile manipulator. Therefore, any value given to $\mathbf{\Lambda}$ will have effects only on the internal structure of the mobile manipulator, and will not affect the final control of the end-effector at all. By using this term, different secondary control objectives can be achieved effectively, as described in the next subsection.

In order to include an analytical saturation of velocities in the mobile manipulator system, both the gain matrix $\mathbf{K_c}\left(\tilde{\boldsymbol{\xi}}\right)$ and the $\tanh(\cdot)$ function are used. The first saturation function limits the image feature error $\tilde{\boldsymbol{\xi}}$ and the second one limits the magnitude of the arbitrary vector $\mathbf{\Lambda}$. The expression $\tanh(\boldsymbol{k_2}\mathbf{\Lambda})$ denotes a component by component operation.

The behavior of the control error $\tilde{\boldsymbol{\xi}}$ is analyzed assuming – by now – perfect velocity tracking, *i.e.* $\mathbf{v} \equiv \mathbf{u}$. With this aim, it is necessary to establish the passivity property for the remaining part of the control system; this is done by considering the following inner product [12],

$$\begin{aligned}\int_0^T \nu_{\tilde{\xi}}^T\left[\mathbf{v}+\mathbf{J}^{\#}\mathbf{J}_o\dot{\mathbf{p}}\right]dt &= \int_0^T \nu_{\tilde{\xi}}^T\left[\mathbf{u}+\mathbf{J}^{\#}\mathbf{J}_o\dot{\mathbf{p}}\right]dt\\ &= \int_0^T \nu_{\tilde{\xi}}^T\left[-\nu_{\tilde{\xi}}-\mathbf{J}^{\#}\mathbf{J}_o\dot{\mathbf{p}}+\left(\mathbf{I}-\mathbf{J}^{\#}\mathbf{J}\right)\boldsymbol{k_1}\tanh\left(\boldsymbol{k_2}\mathbf{\Lambda}\right)+\mathbf{J}^{\#}\mathbf{J}_o\dot{\mathbf{p}}\right]dt\\ &= -\int_0^T \nu_{\tilde{\xi}}^T\nu_{\tilde{\xi}}dt+\int_0^T \nu_{\tilde{\xi}}^T\left(\mathbf{I}-\mathbf{J}^{\#}\mathbf{J}\right)\boldsymbol{k_1}\tanh\left(\boldsymbol{k_2}\mathbf{\Lambda}\right)dt. \qquad (11)\end{aligned}$$

Replacing $\nu_{\tilde{\xi}} = \mathbf{J}^T\mathbf{K_c}\left(\tilde{\boldsymbol{\xi}}\right)\tilde{\boldsymbol{\xi}}$ in the above equation it is obtained

$$\int_0^T \nu_{\tilde{\xi}}^T\left[\mathbf{v}+\mathbf{J}^{\#}\mathbf{J}_o\dot{\mathbf{p}}\right]dt = -\int_0^T \nu_{\tilde{\xi}}^T\nu_{\tilde{\xi}}dt \qquad (12)$$

since $\mathbf{J}\left(\mathbf{I}-\mathbf{J}^{\#}\mathbf{J}\right)=\mathbf{0}$. Therefore, for any $\beta_1 \geq 0$ it holds,

$$-\int_0^T \nu_{\tilde{\xi}}^T\left[\mathbf{v}+\mathbf{J}^{\#}\mathbf{J}_o\dot{\mathbf{p}}\right]dt \geq -\beta_1+\int_0^T\left\|\nu_{\tilde{\xi}}\right\|^2 dt. \qquad (13)$$

Thus, it can now be concluded that mapping $\left(-\nu_{\tilde{\xi}}\right) \rightarrow \left[\mathbf{v}+\mathbf{J}^{\#}\mathbf{J}_o\dot{\mathbf{p}}\right]$ is strictly input passive [14]. This way, the proposed control system is made up by the interconnection of passive systems, as Fig. 4 shows.

By adding the equations related to the passivity properties of the interconnected system: (9) and (13), it is obtained

$$0 \geq -V_1(0)-\beta_1+\int_0^T\left\|\nu_{\tilde{\xi}}\right\|^2 dt \Rightarrow \int_0^T\left\|\nu_{\tilde{\xi}}\right\|^2 dt \leq \beta \qquad (14)$$

with $\beta = V_1(0)+\beta_1$. From (14) it can be concluded that $\nu_{\tilde{\xi}} \in L_2$. Furthermore, because of the definition of $\mathbf{K_c}\left(\tilde{\boldsymbol{\xi}}\right)$ and assuming that the matrix $\mathbf{J}$ is bounded away from any singularity, it can be verified that $\nu_{\tilde{\xi}} \in L_\infty$.

On the other hand, it can also be verified that,

$$\dot{\nu}_{\tilde{\xi}} = \dot{\mathbf{J}}^T\mathbf{K_c}\left(\tilde{\boldsymbol{\xi}}\right)\tilde{\boldsymbol{\xi}}+\mathbf{J}^T\dot{\mathbf{K}}_{\mathbf{c}}\left(\tilde{\boldsymbol{\xi}}\right)\tilde{\boldsymbol{\xi}}+\mathbf{J}^T\mathbf{K_c}\left(\tilde{\boldsymbol{\xi}}\right)\dot{\boldsymbol{\xi}} \qquad (15)$$

remains bounded since, $\mathbf{u} \in L_\infty$ (considering that $\dot{\mathbf{p}} \in L_\infty$), which implies that $\mathbf{v} \in L_\infty$ because of the assumption of perfect velocity tracking, then from image features model (13) it is obvious that $\dot{\boldsymbol{\xi}} \in L_\infty$. Therefore, since $\nu_{\tilde{\xi}} \in L_2 \cap L_\infty$ and $\dot{\nu}_{\tilde{\xi}} \in L_\infty$ it can be concluded by Barbalat's lemma that $\nu_{\tilde{\xi}} \rightarrow \mathbf{0}$ with $t \rightarrow \infty$, which also implies that,

$$\tilde{\boldsymbol{\xi}}(t) \rightarrow \mathbf{0} \quad \text{with } t \rightarrow \infty.$$

It is important to note that the controller design has been made under the assumption of non-singular Jacobian matrix. If this Jacobian matrix becomes singular then it will not be possible to

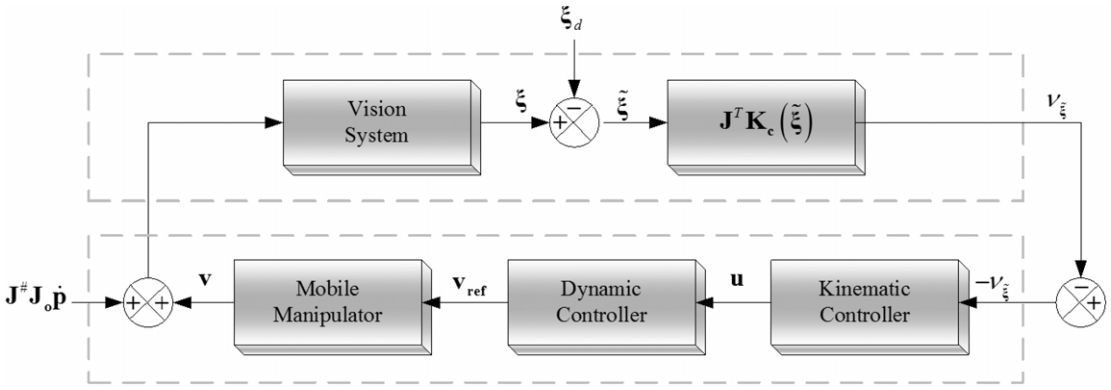

Fig. 5. Dynamic control system block diagram.

calculate the control action (10), losing the control of the robotic system. Therefore, in the next subsection, it will be explained how the redundancy of the mobile manipulator can be used in order to reduce the possibility of attaining a singular configuration.

3.3. Secondary control objectives

The redundancy of mobile manipulators can be effectively used for the achievement of additional performances such as: avoiding obstacles in the workspace, avoiding singular configuration, keeping image features in the field of view, or to optimize various performance criteria. In this work two different secondary objectives are considered: the avoidance of obstacles by the mobile platform and the singular configuration prevention through the system's manipulability control [31]. To this aim, a convenient definition for the vector $\mathbf{\Lambda}$ is used [29],

$$\mathbf{\Lambda} = \begin{bmatrix} -u_{obs} & \omega_{obs} & f_1\left(\tilde{\theta}_1\right) & \cdots & f_{na}\left(\tilde{\theta}_{na}\right) \end{bmatrix}^T. \tag{16}$$

First and second elements of vector $\mathbf{\Lambda}$ represent the linear and angular velocities for the mobile platform. These velocities make the robot capable to avoid obstacles in which maximum height does not interfere with the robotic arm. Therefore the arm can track the object while the mobile platform avoids the obstacle by resourcing to the null space configuration. The angular velocity and the linear velocity of the mobile platform will be affected by a fictitious repulsion force [29]. This force depends on the incidence angle on the obstacle α, and the distance d to the obstacle. This way, the following control velocities are used [29]:

$$u_{obs} = Z^{-1}\left(k_{uobs}\left(d_0 - d\right)\left[\frac{\pi}{2} - |\alpha|\right]\right) \tag{17}$$

$$\omega_{obs} = Z^{-1}\left(k_{\omega obs}\left(d_0 - d\right)\operatorname{sign}\left(\alpha\right)\left[\frac{\pi}{2} - |\alpha|\right]\right) \tag{18}$$

where d is the distance between the robot and the obstacle, d_0 is the distance at which the obstacle starts to be avoided, k_{uobs} and $k_{\omega obs}$ are positive gains, Z represents the mechanical impedance characterizing the robot-environment interaction, and α is the incidence angle on the obstacle.

The rest of the elements of vector $\mathbf{\Lambda}$ represent joint velocities for the robotic arm calculated as functions of joint displacement errors,

$$f_i\left(\tilde{\theta}_i\right) = k_{\Lambda i}\left(\tilde{\theta}_i\right) \quad \text{with } i = 1, \ldots, ma \tag{19}$$

where $\tilde{\theta}_i = \theta_{id} - \theta_i$; $k_{\Lambda i} > 0$. This way, the robotic arm joints will be pulled to the desired θ_{id} values that maximize the manipulability of the mobile manipulator [31]. This way, if the mobile manipulator maintains a high manipulability while performing its movements, then the possibility of attaining a singular configuration is reduced.

3.4. Dynamic compensation controller design

The proposed kinematic controller presented in Section 3.2 assumes perfect velocity tracking, *i.e.* $\mathbf{v} \equiv \mathbf{u}$. Nevertheless, this is not true in real contexts, mainly because of the dynamical effects that could not be disregarded when high-speed movements or heavy load transportation are required. Therefore, it becomes essential in some tasks to consider the mobile manipulator dynamics, in addition to its kinematics. Then, the objective of the dynamic compensation controller is to compensate for the dynamics of the mobile manipulator robot, thus reducing the error between the desired velocity and the actual velocity of the robot. This controller receives as inputs the desired velocities calculated by the kinematic controller, and generates velocity references for the mobile manipulator robot, see (Fig. 5). Hence, relaxing the perfect velocity tracking assumption, the velocity error is defined as, $\tilde{\mathbf{v}}(t) = \mathbf{v}(t) - \mathbf{u}(t)$. This velocity error motivates the dynamic compensation process. Therefore the following control law is proposed,

$$\mathbf{v_{ref}} = \mathbf{M}\left(\mathbf{q}\right)\left(\dot{\mathbf{u}} - \mathbf{K_D}\tilde{\mathbf{v}}\right) + \mathbf{C}\left(\mathbf{q}, \mathbf{v}\right)\mathbf{v} + \mathbf{g}\left(\mathbf{q}\right) \tag{20}$$

where $\mathbf{K_D}$ is a symmetric and positive definite matrix, and

$$\mathbf{v_{ref}} = \begin{bmatrix} u_{ref} & \omega_{ref} & \dot{\theta}_{1ref} & \dot{\theta}_{2ref} & \cdots & \dot{\theta}_{maref} \end{bmatrix}^T.$$

In order to obtain the closed-loop equation, (20) is replaced in the robot dynamics (1),

$$\mathbf{0} = \dot{\tilde{\mathbf{v}}} + \mathbf{K_D}\tilde{\mathbf{v}}. \tag{21}$$

Now, it is important to prove some properties of the velocity error signal $\tilde{\mathbf{v}}$ in order to prove again the asymptotic convergence to zero of the features error. With this aim, a positive definite function is considered: $V_2\left(\tilde{\mathbf{v}}\right) = \frac{1}{2}\tilde{\mathbf{v}}^T\tilde{\mathbf{v}}$. Then, replacing (21) into the time derivative of V_2, it is obtained,

$$\dot{V}_2\left(\tilde{\mathbf{v}}\right) = -\tilde{\mathbf{v}}^T\mathbf{K_D}\tilde{\mathbf{v}} < 0. \tag{22}$$

Thus, since $\dot{V}_2$ is negative definite, it can now be concluded that the velocity error $\tilde{\mathbf{v}} \in L_\infty$ and consequently $\mathbf{v} \in L_\infty$ since also $\mathbf{u} \in L_\infty$.

Now, integrating $\dot{V}_2$ on the interval $[0, T]$ it is obtained,

$$\int_0^T \dot{V}_2 dt = \int_0^T -\tilde{\mathbf{v}}^T\mathbf{K_D}\tilde{\mathbf{v}}dt = V_2(T) - V_2(0) - \int_0^T \tilde{\mathbf{v}}^T\mathbf{K_D}\tilde{\mathbf{v}}dt \geq -V_2(0). \tag{23}$$

Or equivalently,

$$\int_0^T \tilde{\mathbf{v}}^T\mathbf{K_D}\tilde{\mathbf{v}}dt \leq V_2(0) \Rightarrow \int_0^T \left\|\tilde{\mathbf{v}}\right\|^2 dt \leq \frac{V_2(0)}{\lambda_{\min}\left(\mathbf{K_D}\right)} \tag{24}$$

being $\lambda_{\min}(\mathbf{K_D})$ the minimum eigen value of $\mathbf{K_D}$. Eq. (24) implies that $\tilde{\mathbf{v}} \in L_2$.

Since a more realistic situation is now considered, in which the robot does not reach instantaneously the desired velocities, *i.e.*, $\mathbf{v}(t) = \tilde{\mathbf{v}}(t) + \mathbf{u}(t)$, inner product (11) should be written as,

$$\begin{aligned}\int_0^T \nu_{\tilde{\xi}}^T \left[\mathbf{v} + \mathbf{J}^{\#}\mathbf{J}_o\dot{\mathbf{p}}\right] dt &= \int_0^T \nu_{\tilde{\xi}}^T \left[\mathbf{u} + \tilde{\mathbf{v}} + \mathbf{J}^{\#}\mathbf{J}_o\dot{\mathbf{p}}\right] dt \\ &= \int_0^T \nu_{\tilde{\xi}}^T \left[-\nu_{\tilde{\xi}} + \tilde{\mathbf{v}}\right] dt \\ &= -\int_0^T \nu_{\tilde{\xi}}^T \nu_{\tilde{\xi}} dt + \int_0^T \nu_{\tilde{\xi}}^T \tilde{\mathbf{v}} dt. \end{aligned} \tag{25}$$

Therefore,

$$-\int_0^T \nu_{\tilde{\xi}}^T \left[\mathbf{v} + \mathbf{J}^{\#}\mathbf{J}_o\dot{\mathbf{p}}\right] dt = \int_0^T \nu_{\tilde{\xi}}^T \nu_{\tilde{\xi}} dt - \int_0^T \nu_{\tilde{\xi}}^T \tilde{\mathbf{v}} dt. \tag{26}$$

By adding previous Eq. (26) with the passivity property of the vision system (9) the following inequality can now be obtained,

$$\begin{aligned} 0 &\geq -V_1(0) + \int_0^T \left\|\nu_{\tilde{\xi}}\right\|^2 dt - \int_0^T \nu_{\tilde{\xi}}^T \tilde{\mathbf{v}} dt \\ \int_0^T \left\|\nu_{\tilde{\xi}}\right\|^2 dt &\leq V_1(0) + \int_0^T \nu_{\tilde{\xi}}^T \tilde{\mathbf{v}} dt. \end{aligned} \tag{27}$$

In addition, Schwartz inequality states that

$$\int_0^T \nu_{\tilde{\xi}}^T \tilde{\mathbf{v}} dt \leq \left\|\nu_{\tilde{\xi}}\right\|_{2,T} \left\|\tilde{\mathbf{v}}\right\|_{2,T}. \tag{28}$$

The above equation can be used to reinforce (27) thus obtaining,

$$\int_0^T \left\|\nu_{\tilde{\xi}}\right\|^2 dt \leq V_1(0) + \left\|\nu_{\tilde{\xi}}\right\|_{2,T} \left\|\tilde{\mathbf{v}}\right\|_{2,T}. \tag{29}$$

Hence, recalling that (24) implies that $\tilde{\mathbf{v}} \in L_2$, it can be concluded from (29) and the definition of $\nu_{\tilde{\xi}}$ that $\nu_{\tilde{\xi}} \in L_2 \cap L_\infty$. With $\mathbf{v} \in L_\infty$, even when the hypothesis of perfect velocity tracking is not considered, $\dot{\nu}_{\tilde{\xi}} \in L_\infty$ can be proved again. Therefore, since $\nu_{\tilde{\xi}} \in L_2 \cap L_\infty$ and $\dot{\nu}_{\tilde{\xi}} \in L_\infty$, by Barbalat's Lemma, $\nu_{\tilde{\xi}} \to \mathbf{0}$ with $t \to \infty$ which implies that,

$$\tilde{\boldsymbol{\xi}}(t) \to \mathbf{0} \quad \text{with } t \to \infty.$$

4. Robustness and L_2-gain performance analysis

The proposed controller presented in previous section considers that the velocity of the object to be followed $\dot{\mathbf{p}}$ is exactly known. Nevertheless, this is not always possible in real context. In practice this velocity will be estimated by using the visual position sensing of the object through, for instance, an $\alpha - \beta$ filter [32,33]. The estimation of the object velocity immediately raises the problem of analyzing the effect of the estimation error on the control errors. In this analysis, the L_2-gain performance criterion will be used.

It is defined the estimation velocity errors of the object,

$$\tilde{\dot{\mathbf{p}}} = \dot{\mathbf{p}} - \hat{\dot{\mathbf{p}}} \tag{30}$$

where $\dot{\mathbf{p}}$ and $\hat{\dot{\mathbf{p}}}$ are the real and estimated velocities of the object, respectively. Furthermore, it is assumed that $\gamma = \mathbf{J}_o\left(\dot{\mathbf{p}} - \hat{\dot{\mathbf{p}}}\right)$ is bounded and,

$$\|\gamma\|_\infty = \sup_{t\in[t_1,T]} \|\gamma(t)\| < \lambda' k_{\min} \tag{31}$$

with $k_{\min} = \min\{k_i\}$, $\lambda' = \varepsilon\lambda$, being $\lambda = \inf_{\mathbf{q},\xi}\left(\lambda_{\min}\left(\mathbf{J}\mathbf{J}^T\right)\right)$ and $0 < \varepsilon < 1$.

First, the following positive definite function is considered,

$$V_1 = \int_0^{\tilde{\xi}} \eta^T \mathbf{K_c}(\eta)\, d\eta \tag{32}$$

and its time derivative on the trajectories of the system is,

$$\dot{V}_1 = \tilde{\boldsymbol{\xi}}^T \mathbf{K_c}\left(\tilde{\boldsymbol{\xi}}\right)\dot{\tilde{\boldsymbol{\xi}}} = \tilde{\boldsymbol{\xi}}^T \mathbf{K_c}\left(\tilde{\boldsymbol{\xi}}\right)\left[\mathbf{J}\mathbf{v} + \mathbf{J}_o\dot{\mathbf{p}}\right]. \tag{33}$$

Consider now the object velocity estimation $\hat{\dot{\mathbf{p}}}$ in the expression for the control action,

$$\mathbf{u} = -\nu_{\tilde{\xi}} - \mathbf{J}^{\#}\mathbf{J}_o\hat{\dot{\mathbf{p}}} + \left(\mathbf{I} - \mathbf{J}^{\#}\mathbf{J}\right)\boldsymbol{k_1}\tanh\left(\boldsymbol{k_2}\boldsymbol{\Lambda}\right) \tag{34}$$

and assuming perfect velocity tracking, *i.e.*, $\mathbf{v} \equiv \mathbf{u}$, the following equation is obtained after introducing (34) into (33),

$$\begin{aligned}\dot{V}_1 = {} & \tilde{\boldsymbol{\xi}}^T \mathbf{K_c}\left(\tilde{\boldsymbol{\xi}}\right) \\ & \times \left[\mathbf{J}\left(-\nu_{\tilde{\xi}} - \mathbf{J}^{\#}\mathbf{J}_o\hat{\dot{\mathbf{p}}} + \left(\mathbf{I} - \mathbf{J}^{\#}\mathbf{J}\right)\boldsymbol{k_1}\tanh\left(\boldsymbol{k_2}\boldsymbol{\Lambda}\right)\right) + \mathbf{J}_o\dot{\mathbf{p}}\right]. \end{aligned} \tag{35}$$

After some manipulations and recalling that $\mathbf{J}\left(\mathbf{I} - \mathbf{J}^{\#}\mathbf{J}\right) = 0$ because of $\mathbf{J}^{\#}$ definition, the following expression is obtained,

$$\begin{aligned}\dot{V}_1 &= -\tilde{\boldsymbol{\xi}}^T \mathbf{K_c}\left(\tilde{\boldsymbol{\xi}}\right)\mathbf{J}\mathbf{J}^T \mathbf{K_c}\left(\tilde{\boldsymbol{\xi}}\right)\tilde{\boldsymbol{\xi}} + \tilde{\boldsymbol{\xi}}^T \mathbf{K_c}\left(\tilde{\boldsymbol{\xi}}\right)\mathbf{J}_o\tilde{\dot{\mathbf{p}}} \\ \dot{V}_1 &\leq -\lambda \left\|\tilde{\boldsymbol{\xi}}^T \mathbf{K_c}\left(\tilde{\boldsymbol{\xi}}\right)\right\|^2 + \left\|\tilde{\boldsymbol{\xi}}^T \mathbf{K_c}\left(\tilde{\boldsymbol{\xi}}\right)\right\| \|\gamma(t)\|. \end{aligned} \tag{36}$$

Eq. (36) implies that a sufficient condition for $\dot{V}_1$ to be negative definite is,

$$\lambda \left\|\tilde{\boldsymbol{\xi}}^T \mathbf{K_c}\left(\tilde{\boldsymbol{\xi}}\right)\right\|^2 > \left\|\tilde{\boldsymbol{\xi}}^T \mathbf{K_c}\left(\tilde{\boldsymbol{\xi}}\right)\right\| \|\gamma(t)\|. \tag{37}$$

Therefore, the signal $\left(\tilde{\boldsymbol{\xi}}^T \mathbf{K_c}\left(\tilde{\boldsymbol{\xi}}\right)\right)$ is ultimately bounded, *i.e.*, for a finite t_1,

$$\left\|\tilde{\boldsymbol{\xi}}^T \mathbf{K_c}\left(\tilde{\boldsymbol{\xi}}\right)\right\| \leq \frac{\|\gamma\|_\infty}{\lambda'}. \tag{38}$$

After t_1 and recalling assumption (31), inequality (38) can be reinforced as,

$$\begin{aligned}\frac{k_{\min}}{1 + \left\|\tilde{\boldsymbol{\xi}}(t)\right\|} \left\|\tilde{\boldsymbol{\xi}}(t)\right\| &\leq \frac{\|\gamma\|_\infty}{\lambda'} \\ \left\|\tilde{\boldsymbol{\xi}}(t)\right\| &\leq \frac{\|\gamma\|_\infty}{\lambda' k_{\min} - \|\gamma\|_\infty}. \end{aligned} \tag{39}$$

The above equation shows that given a higher bound for $\left(\tilde{\boldsymbol{\xi}}^T \mathbf{K_c}\left(\tilde{\boldsymbol{\xi}}\right)\right)$, a higher bound for $\tilde{\boldsymbol{\xi}}(t)$ also exists. These bounds (38) and (39) can be used for reinforcing inequality (36) as follows,

$$\dot{V}_1 \leq -\lambda' \left(\frac{\lambda' k_{\min} - \|\gamma\|_\infty}{\lambda'}\right)^2 \left\|\tilde{\boldsymbol{\xi}}(t)\right\|^2 + \frac{\|\gamma(t)\|^2}{\lambda'}. \tag{40}$$

Integrating (40) on the interval $[t_1, T]$,

$$\begin{aligned} V_1(T) - V_1(t_1) &\leq -\frac{\left(\lambda' k_{\min} - \|\gamma\|_\infty\right)^2}{\lambda'} \int_{t_1}^T \left\|\tilde{\boldsymbol{\xi}}(t)\right\|^2 dt \\ &\quad + \frac{1}{\lambda'} \int_{t_1}^T \|\gamma(t)\|^2 dt \\ -V_1(t_1) &\leq -\frac{\left(\lambda' k_{\min} - \|\gamma\|_\infty\right)^2}{\lambda'} \int_{t_1}^T \left\|\tilde{\boldsymbol{\xi}}(t)\right\|^2 dt \\ &\quad + \frac{1}{\lambda'} \int_{t_1}^T \|\gamma(t)\|^2 dt \end{aligned} \tag{41}$$

Fig. 6. Experimental setup.

and reorganizing (41), the following equation is obtained,

$$\int_{t_1}^{T} \left\| \tilde{\boldsymbol{\xi}}(t) \right\|^2 dt \leq \varsigma^2 \int_{t_1}^{T} \|\gamma(t)\|^2 dt + \zeta \tag{42}$$

with $\varsigma = \frac{1}{\lambda' k_{\min} - \|\gamma\|_\infty}$, and $\zeta = \lambda' \varsigma^2 V_1(t_1)$.

Eq. (39) shows that visual control errors will be finally bounded when errors in the object velocity estimation are considered. Even more, an important conclusion can be obtained from (42): After a finite time t_1, the designed control system has finite L_2-gain $\leq \varsigma$ from the disturbance to the control errors, hence it will be robust in the sense of L_2 performance criterion [14,17,19,22] when considering γ as an external disturbance of the control system. In this context, parameter ς can be considered as an indicator of the control system performance in presence of estimation errors.

Note that same conclusion can be obtained when considering the dynamic compensation controller. In this case, the velocity error $\tilde{\mathbf{v}}$ should be included as part of the external disturbance γ.

5. Experimental results

In order to evaluate the performance of the proposed controller, several experiments were carried out using the proposed visual control for 3D target tracking by a mobile manipulator. The 6 DOF experimental system used in the experiments is shown in Fig. 6, which is composed of a non-holonomic mobile platform PIONEER 3AT, a laser rangefinder mounted on it, a robotic arm CYTON Alpha 7 DOFs (only 3 DOF of the 7 available DOFs are used in the experiment), and a JMK Mini CMOS Camera (model: JK-805) with 1/3″ Video Sensor, resolution: 628 × 582 pixels. The laser range finder is used only for the obstacles detection. The target to be tracked is mounted on another mobile platform PIONEER 3DX as Fig. 6 shows.

The positions of the arm joints that maximize the arm's manipulability are obtained off-line through numeric simulation. This way, the desired joint angles are: $\theta_{1d} = 0$ rad, $\theta_{2d} = 0.6065$ rad, and $\theta_{3d} = 1.2346$ rad. For all the experiments the initial robot configuration is $\mathbf{q} = \begin{bmatrix} 0\,\text{m} & 0\,\text{m} & 0\,\text{rad} & 0\,\text{rad} & 0\,\text{rad} & 0\,\text{rad} \end{bmatrix}^T$. Finally, gain matrices of the controller are set as: $k_{\Lambda i} = 1$; $k_{uobs} = 0.5$; $k_{\omega obs} = 0.9$; $\mathbf{K_D} = \text{diag}\begin{pmatrix} 0.3 & 0.3 \end{pmatrix}$; $\boldsymbol{k_1} = \text{diag}\begin{pmatrix} 0.7 & 1 & 0.1 & 0.1 & 0.1 \end{pmatrix}$; $\boldsymbol{k_2} = \text{diag}\begin{pmatrix} 0.2 & 0.2 & 0.2 & 0.2 & 0.2 \end{pmatrix}$ and $k_i = 0.15$. Note that dynamic compensation is performed for the mobile platform only since, in used lab equipment, it represents the most significant dynamics of the whole mobile manipulator system. Additionally, the joints information needed for the manipulability secondary objective is obtained from the inner sensors of the robotic arm.

Experiment 1: In the first experiment the target moves along a straight path for about 20 s and then it stops abruptly. The purpose of this experiment is to evaluate the performance of the proposed control system with large errors in the target velocity estimation. Initial image feature vector is $\boldsymbol{\xi}(0) = \begin{bmatrix} -150 & 20 & -100 \end{bmatrix}^T$ expressed in pixels and the desired features vector is set as $\boldsymbol{\xi}_d = \begin{bmatrix} 0 & 60 & -60 \end{bmatrix}^T$. Figs. 7–10 show the results of the first experiment. Fig. 7 shows that the control errors $\tilde{\boldsymbol{\xi}}(t)$ are ultimately bounded with final values close to zero, *i.e.*, achieving final feature errors $\max\left(\left|\tilde{\xi}_i\right|\right) < 8$ pixels. Figs. 8 and 9 show the control actions of the mobile manipulator; while Fig. 10 represents the norm of the estimated object's velocity. Notice that even with large velocity estimation errors, like the errors which appear at the beginning of the experiment, the control errors remain bounded.

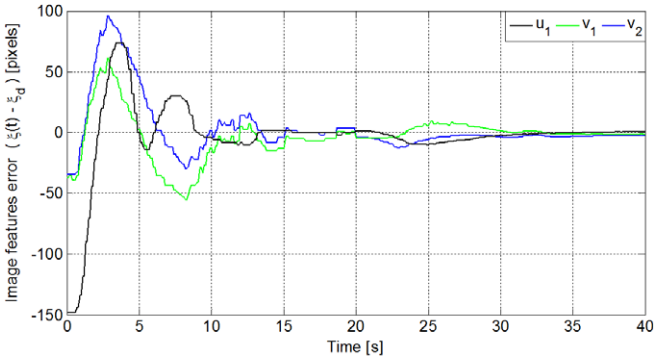

Fig. 7. Time evolution of control errors $\tilde{\boldsymbol{\xi}}(t)$.

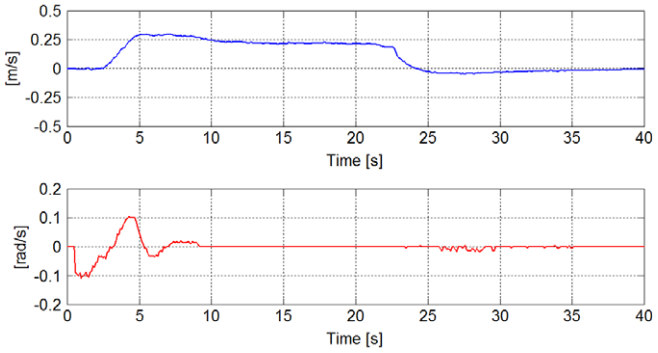

Fig. 8. Velocities commands to the mobile platform.

Experiment 2: In this experiment, a more complex scenario is adopted. The target moves along a non-straight path and a static obstacle should be avoided by the robot. Also the singular configuration prevention through the system's manipulability control is considered. It is assumed that the obstacle is placed up to a maximum height that it does not interfere with the vision camera, so that the end-effector can follow the target object

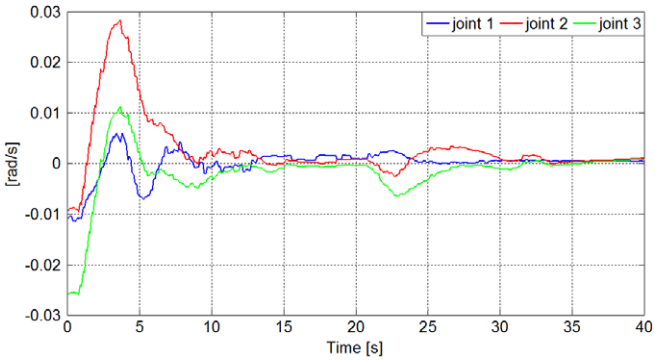

Fig. 9. Joint velocity commands to the robotic arm.

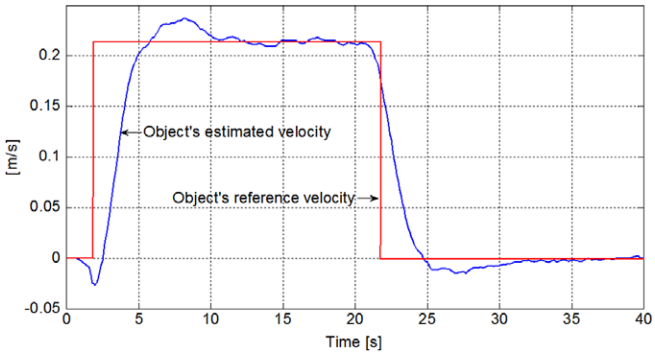

Fig. 10. Norm of the estimated object's velocity.

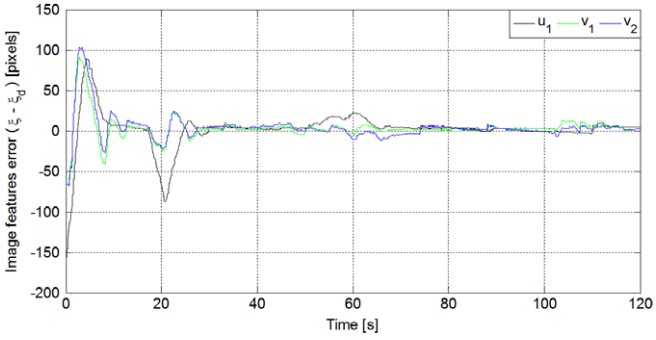

Fig. 11. Time evolution of control errors $\tilde{\xi}(t)$.

even when the platform is avoiding the obstacle. Hence, the task is divided into two different control objectives, *i.e.*, a principal objective: *moving target object tracking*; and secondary objectives, achieved by taking advantage of the redundancy of the mobile manipulator as explained in Section 3.3. Initial image feature vector is $\boldsymbol{\xi}(0) = \begin{bmatrix} -150 & 0 & -115 \end{bmatrix}^T$ expressed in pixels and the desired features vector is set as $\boldsymbol{\xi}_d = \begin{bmatrix} 0 & 60 & -60 \end{bmatrix}^T$. Figs. 11–14 show the results of the experiment. Fig. 11 shows the evolution of the image control errors. Figs. 12 and 13 show the control actions applied for the platform and for the robotic arm respectively. Finally, Fig. 14 shows the stroboscopic movement on the X–Y–Z space, it is based on the experimental data. In Figs. 11–13 (for 17 s $< t <$ 32 s approximately) it can be observed the actions taken by the controller in order to avoid the obstacle while tracking the target. The obstacle avoidance can also be seen in Fig. 14 at instant 3. Note that after avoiding the obstacle, the robotic arm returns to its maximum manipulability configuration according to this specific secondary objective. In Fig. 11 it can be observed that the control errors remain bounded even when the obstacle is

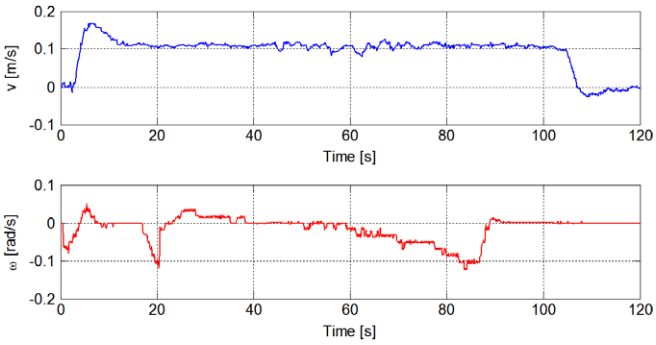

Fig. 12. Velocities commands to the mobile platform.

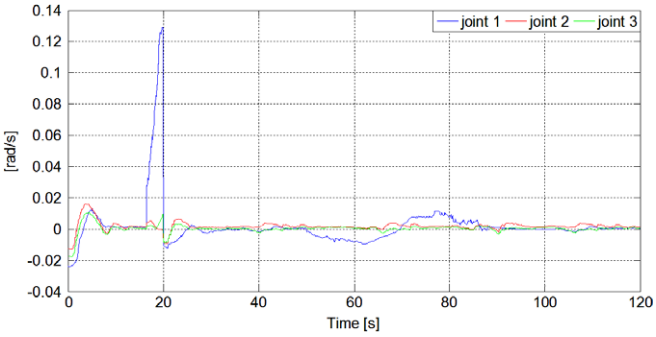

Fig. 13. Joint velocity commands to the robotic arm.

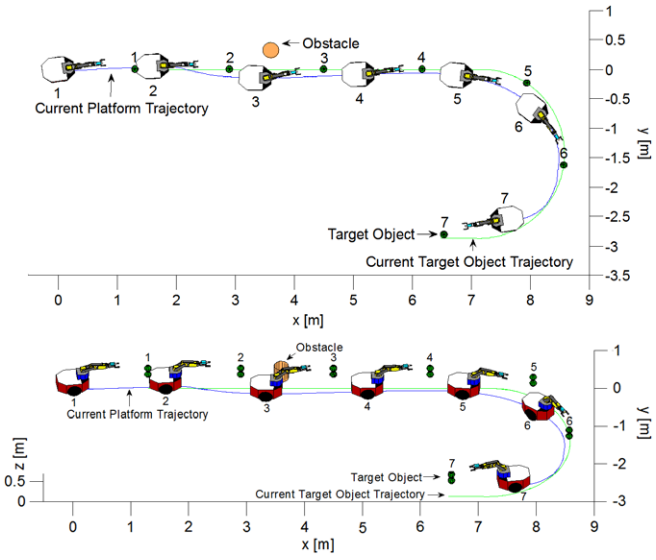

Fig. 14. Movement of the mobile manipulator based on the experimental data. The position of the mobile manipulator and the position of the target at the same instant are shown. Seven different time instants are depicted.

avoided and in spite of the errors in the estimation of the target velocity. The good performance of the proposed controller can be concluded from the obtained results.

Experiment 3: In the third experiment the target moves along a straight path, as in experiment 1, with constant linear velocity and then it stops. The purpose of this experiment is to evaluate the performance of the proposed control system under the presence of uncertainties in the kinematic model of the robotic system. With this aim, errors of 20% in kinematic model have been introduced. Initial image feature vector is $\boldsymbol{\xi}(0) = \begin{bmatrix} -212 & 11 & -137 \end{bmatrix}^T$ expressed in pixels and the desired features vector is set as

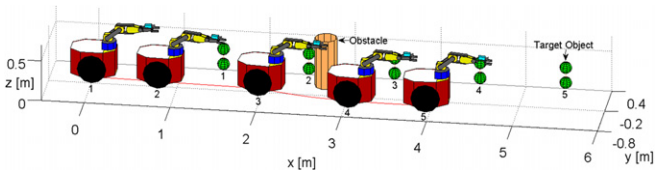

Fig. 15. Movement of the mobile manipulator based on the experimental data. The position of the mobile manipulator and the position of the target at the same instant are shown. Five different time instants are depicted.

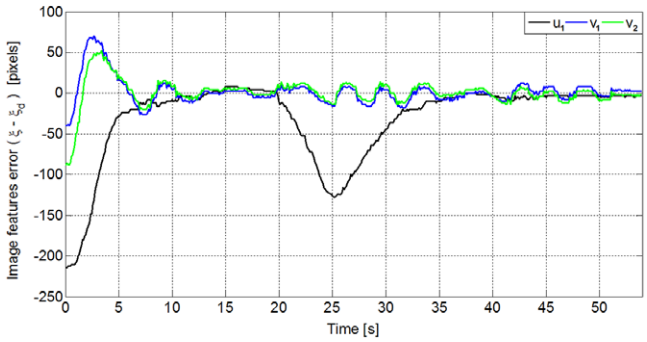

Fig. 16. Time evolution of control error $\tilde{\xi}(t)$.

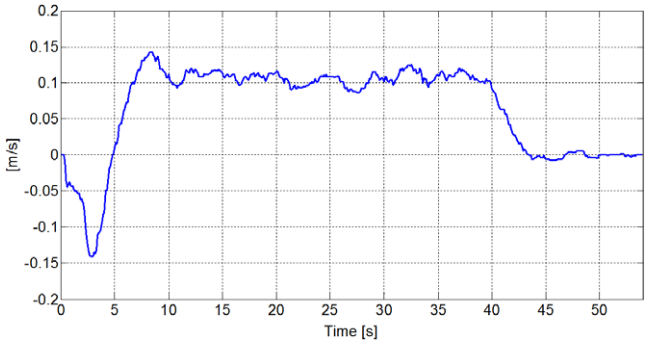

Fig. 17. Velocity commands to the mobile platform.

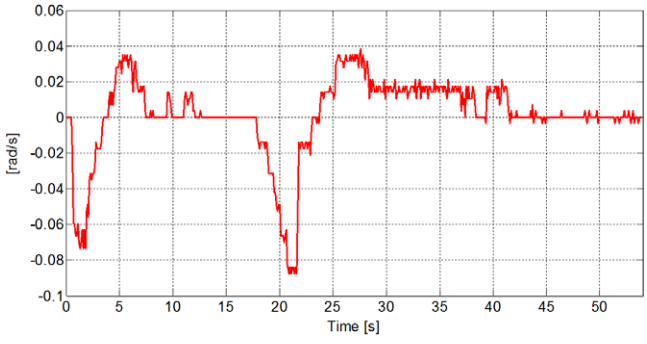

Fig. 18. Velocity commands to the mobile platform.

$\boldsymbol{\xi}_d = \begin{bmatrix} 0 & 50 & -50 \end{bmatrix}^T$. Results obtained in this experiment are shown in Figs. 15–19. In Figs. 18 and 19 (18 s $< t <$ 30 s approximately) it can be observed that the end-effector tracks the moving target object while avoiding the obstacle. Fig. 15 shows the reconstruction of the stroboscopic movement on the X–Y–Z space. Fig. 16 shows that the control errors $\tilde{\boldsymbol{\xi}}(t)$ remain bounded even with the errors introduced in the kinematic model. It can be seen in Fig. 16 how the performance of the control system is deteriorated with respect to the others experiments but still having an

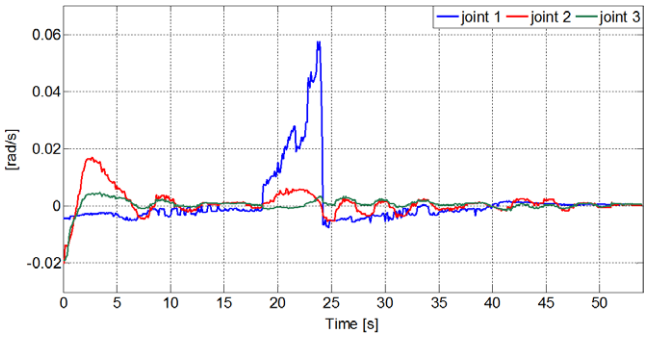

Fig. 19. Joint velocity commands to the robotic arm.

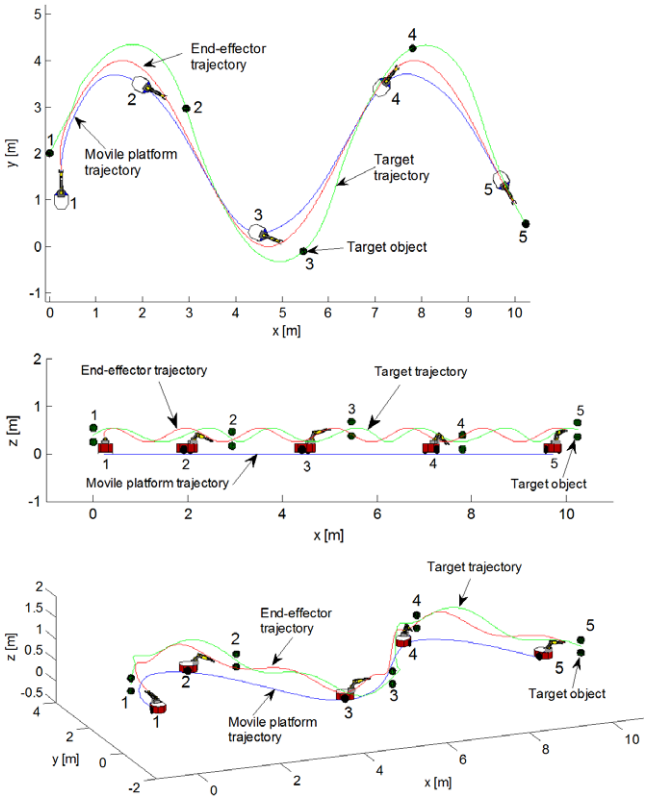

Fig. 20. Movement of the mobile manipulator. The position of the mobile manipulator and the position of the target at the same instant are shown. Five different time instants are depicted.

acceptable performance. Figs. 17–19 show the control actions of the mobile manipulator.

Experiment 4: This experiment is a simulation result carried out in order to evaluate the system performance when the target performs a movement in the 3D space. That is, it does not only describe a trajectory only in the X–Y plane but it also changes its z-coordinate. Simulation has been performed including the dynamical model of the mobile manipulator and considering perfect knowledge of the object's velocity and perfect knowledge of the system's dynamic and kinematic models. In this simulation, $\boldsymbol{\xi}(0) = \begin{bmatrix} 212 & -50 & -120 \end{bmatrix}^T$ and $\boldsymbol{\xi}_d = \begin{bmatrix} 0 & 50 & -50 \end{bmatrix}^T$. Obtained results are shown in Figs. 20–23. Fig. 20 shows the stroboscopic movement on the X–Y plane, the X–Z plane as well as on the X–Y–Z space. Fig. 21 shows the time evolution of the features error, where it can be seen that they converge to zero asymptotically when the target describes its movement in the 3D space. Figs. 22 and 23 show the control actions applied for the platform and for the robotic arm respectively.

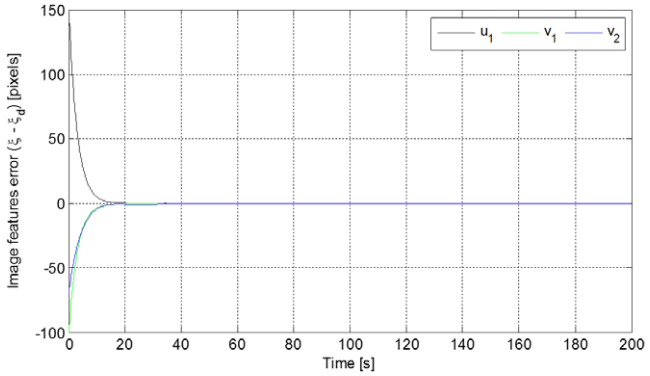

Fig. 21. Time evolution of control error $\tilde{\xi}(t)$.

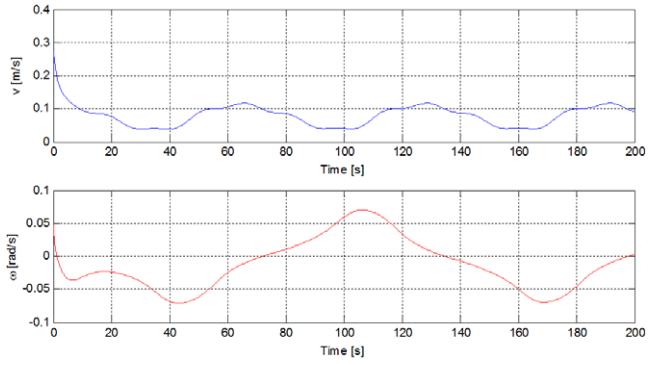

Fig. 22. Velocities commands to the mobile platform.

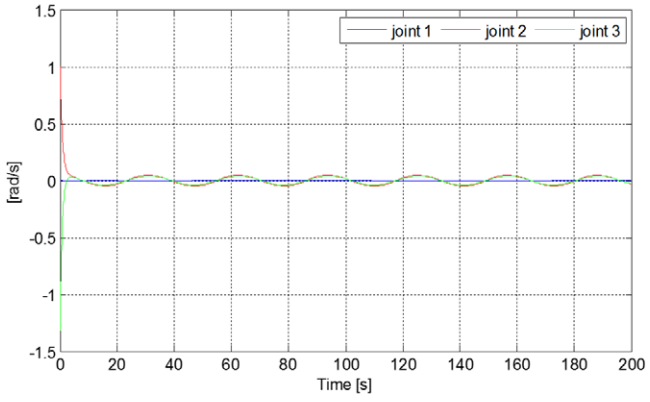

Fig. 23. Joint velocity commands to the robotic arm.

6. Conclusions

In this paper, a 3D passivity-based visual controller for mobile manipulator with eye-in-hand configuration was presented. Also, it has been considered the redundancy of the mobile manipulator system to comply with the objectives of obstacle avoidance by the mobile platform and the singular configuration prevention through the system's manipulability control. The design of the whole controller was based on two cascaded subsystems. First, a kinematics-based controller has been proposed and the asymptotical convergence to zero of the control errors has been proved assuming perfect velocity tracking. Then, a more realistic situation when a joint velocity error appears has been considered and a dynamics-based velocity controller has been designed to prove again the convergence to zero of the image features error under this condition. The dynamics based controller receives the velocity references values from the kinematics-based one. The stability proof of the proposed system is based on its passivity properties and the input–output systems theory. Finally, estimation errors on the object velocity have been considered on a robustness analysis concluding that control errors are ultimately bounded in presence of these estimation errors. Even more, it has been proved that the proposed system has L_2-gain after a finite time when the object velocity estimation error is considered as an external disturbance of the system. Therefore, after a finite time, the system will be robust to these errors following the L_2-gain performance criterion. The performance of the proposed controller is shown through both simulations and real experiments.

Acknowledgments

Authors thanks to Consejo Nacional de Investigaciones Científicas y Técnicas of Argentina (CONICET), PIP2012-2014 N° 11220110100223; Ministerio de Ciencia e Innovación of Spain, DPI2010-20863; and Universidad Nacional de San Juan of Argentina, UNSJ2014-2015 N° 21I-267, for partially supporting this research.

References

[1] O. Khatib, Mobile manipulation: the robotic assistant, Robot. Auton. Syst. 26 (2–3) (1999) 175–183.
[2] Y. Das, K. Russell, N. Kircanski, A. Goldenberg, An articulated robotic scanner for mine detection—a novel approach to vehicle mounted systems, in: Proc. of the SPIE Conf.: Detection and Remediation Technologies for Mines and Minelike Targets IV, Orlando, USA, 1999.
[3] A. Muis, Ohnishi, Eye-to-hand approach on eye-in-hand configuration within real-time visual servoing, IEEE/ASME Trans. Mechatronics 10 (4) (2005) 404–410.
[4] Y. Wang, H. Lang, C. de Silva, A hybrid visual servo controller for robust grasping by wheeled mobile robots, IEEE/ASME Trans. Mechatronics 15 (5) (2009) 757–769.
[5] Y. Zhang, M. Mehrandezh, Visual servoing of a 5-DOF mobile manipulator using a panoramic vision system, in: Canadian Conf. on Electrical and Computer Engineering, 2007, pp. 453–456.
[6] H.J. Lee, M.C. Lee, Color-based visual servoing of a mobile manipulator with stereo vision, in: Proc. of the 17th World Congress of the Int. Federation of Aut. Control, Seoul, Korea, 2008, pp. 2359–2364.
[7] De Luca, G. Oriolo, P. Giordano, Image-based visual servoing schemes for nonholonomic mobile manipulators, Robotica 25 (2) (2007) 131–145.
[8] Hideaki Tai, Toshiyuki Murakami, A control of two wheels driven redundant mobile manipulator using a monocular camera system, Int. J. Intell. Syst. Technol. Appl. 8 (2009) 361–381.
[9] L. Sun, M. Zhang, Based on Kalman filter the mobile manipulator non-calibration free dynamic target tracking technology research, in: Proc. of The IEEE 2009 Int. Conf. on Electronic Computer Technology, Macau, China, 2009, pp. 610–614.
[10] M. Kazemi, K. Gupta, M. Mehrandezh, Path-planning for visual servoing: a review and issues, in: G. Chesi, K. Hashimoto (Eds.), Visual Servoing via Advanced Numerical Methods, in: Lecture Notes in Control and Information Sciences, vol. 401, Springer-Verlag, Berlin, Heidelberg, 2010, pp. 109–207 (Chapter 11).
[11] V. Andaluz, R. Carelli, L. Salinas, J.M. Toibero, F. Roberti, Visual control with adaptive dynamical compensation for 3D target tracking by mobile manipulators, Mechatronics 22 (4) (2012) 491–502.
[12] C.I. Bynes, A. Isidori, J. Willems, Passivity, feedback equivalence, and the global stabilization of minimum phase nonlinear systems, IEEE Trans. Automat. Control 36 (11) (1991) 1228–1240.
[13] R. Ortega, A. Loria, R. Kelly, L. Praly, On passivity based output feedback global stabilization of Euler–Lagrange systems, Internat. J. Robust Nonlinear Control 5 (4) (1995) 313–324.
[14] Van Der Schaft, L_2-Gain and Passivity Techniques in Nonlinear Control, Springer-Verlag, London, 2000.
[15] T. Murao, H. Kawai, M. Fujita, Passivity-based dynamic visual feedback control with a movable camera, in: Proc. of IEEE Int. Conf. on Decision and Control, Tokio, Japan, December, 2005.
[16] H. Kawai, M. Toshiyuki, M. Fujita, Image-based dynamic visual feedback control via passivity approach, in: Proc. of the IEEE Int. Conf. on Control Applications, Munich, Germany, October, 2006.
[17] M. Fujita, H. Kawai, M.W. Spong, Passivity-based dynamic visual feedback control for three dimensional target tracking: stability and L_2-gain performance analysis, IEEE Trans. Control Syst. Technol. 15 (1) (2007) 40–52.

[18] Kugi, C. Ott, A. Albu-Schaffer, G. Hirzinger, On the passivity-based impedance control of flexible joint robots, IEEE Trans. Robot. 24 (2) (2008) 416–429.
[19] Soria, F. Roberti, R. Carelli, J.M. Sebastián, Visual servo control of a robot manipulator based on passivity, RIAI 5 (4) (2008) 54–61 (in Spanish: Control Servo-Visual De Un Robot Manipulador Planar Basado En Pasividad).
[20] Lee, Passivity-based switching control for stabilization of wheeled mobile robots, in: Proc. of the Robotics Science and Systems, Atlanta, Georgia, USA, June, 2007.
[21] M.I. El-Hawwary, M. Maggiore, Global path following for the unicycle and other results, in: Proc. of American Control Conference, Seattle, USA, June 2008.
[22] B. Morales, F. Roberti, J.M. Toibero, R. Carelli, Passivity based visual servoing of mobile robots with dynamics compensation, Mechatronics 22 (4) (2012) 481–590.
[23] Ihle, M. Arcak, T. Fossen, Passivity-based designs for synchronized path-following, Automatica 43 (9) (2007) 1508–1518.
[24] M. Arcak, Passivity as a design tool for group coordination, IEEE Trans. Automat. Control 52 (8) (2007) 1380–1390.
[25] Y. Igarashi, T. Hatanaka, M. Fujita, M.W. Spong, Passivity-Based 3D attitude coordination: convergence and connectivity, in: Proc. of IEEE Int. Conf. on Decision and Control, New Orleans, LA, USA, 2007.
[26] M.W. Spong, J.K. Holm, D.J. Lee, Passivity-based control of biped locomotion, IEEE Robot. Autom. Mag. 14 (2) (2007) 30–40.
[27] Farkhatdinov, J. Ryu, J. Poduraev, A feasibility study of time-domain passivity approach for bilateral teleoperation of mobile manipulator, in: Proc. of Int. Conf. on Control, Automation and Systems, Seoul, Korea, October, 2008.
[28] T. Shibata, T. Murakami, A null space control of two wheels driven mobile manipulator using passivity theory, IEEE Trans. Ind. Appl. 127 (11) (2007) 1109–1116.
[29] V. Andaluz, F. Roberti, J.M. Toibero, R. Carelli, Adaptive unified motion control of mobile manipulators, Control Eng. Pract. 20 (12) (2012) 1337–1352.
[30] Y.M. Hu, B.H. Guo, Modeling and motion planning of a three-link wheeled mobile manipulator, in: Proc. of the Int. Conf. on Control, Automation and Vision, Guangzhou, China, 2004, pp. 993–998.
[31] B. Bayle, J.Y. Fourquet, Manipulability analysis for mobile manipulators, in: Proc. of IEEE Int. Conf. on Robotics and Automation, Seoul, Korea, May 2001.
[32] R. Carelli, J. Santos-Victor, F. Roberti, S. Tosetti, Direct visual tracking control of remote cellular robots, Robot. Auton. Syst. 54 (10) (2006) 805–814.
[33] P. Kalata, The tracking index: a generalized parameter for α-β and α-β-γ target trackers, IEEE Trans. Aerosp. Electron. Syst. 20 (2) (1994) 174–182.

Víctor H. Andaluz was born in Ambato, Ecuador in 1984. He graduated in Electronics and Control Engineering from the EPN, Ecuador in 2008, and obtained a Ph.D. degree in Control Systems Engineering from the National University of San Juan, Argentina in 2011.

He is currently Lecture at the Polytechnic University of Ambato, Ecuador. His research interests are mobile robots, mobile manipulators and miniature helicopters.

Flavio Roberti was born in Buenos Aires, Argentina in 1978. He graduated in Engineering from the National University of San Juan, Argentina in 2004, and obtained a Ph.D. degree in Control Systems Engineering from the National University of San Juan, Argentina in 2009.

He is currently Associate Professor at the National University of San Juan and Researcher of the National Council for Scientific and Technical Research (CONICET, Argentina). His research interests are robotics; wheeled mobile robots; mobile manipulators, visual servoing and passivity based visual control.

Lucio Salinas was born in San Juan, Argentina in 1982. He graduated in Engineering from the National University of San Juan, Argentina in 2008.

He is currently Ph.D. student in Control Systems Engineering at the National University of San Juan (Argentina), with a grant from the CONICET (National Council for Scientific and Technical Research). His research interests are robotics, nonlinear control, teleoperation systems and unmanned aerial vehicles.

Juan M. Toibero was born in Santa Fe, Argentina in 1977. He graduated in Engineering from the National Technological University of Parana, Argentina in 2002, and obtained a Ph.D. degree in Control Systems Engineering from the National University of San Juan, Argentina in 2007.

He is currently Associate Professor at the National University of San Juan and Assistant Researcher of the National Council for Scientific and Technical Research (CONICET, Argentina). His research interests are robotics; wheeled mobile robots; switched, hybrid and nonlinear control methods applied to automatic control, and artificial intelligence applied to automatic control.

Ricardo Carelli was born in San Juan, Argentina in 1952. He graduated in Engineering from the National University of San Juan, Argentina in 1976, and obtained a Ph.D. degree in Electrical Engineering from the National University of Mexico (UNAM) in 1989.

He is currently Full Professor at the National University of San Juan and Senior Researcher of the National Council for Scientific and Technical Research (CONICET, Argentina). He is Director of the Institute of Automatics, National University of San Juan. He2222 also coordinates the Ph.D. and Master Programs in Control Engineering at the same university. His research interests are robotics, manufacturing systems, adaptive control and artificial intelligence applied to automatic control.

He is also a member of the Argentine Association of Automatic Control (AADECA-IFAC).